Synthesis gas production via the biogas reforming reaction over Ni/MgO-Al_2O_3 and Ni/CaO-Al_2O_3 catalysts

N.D. Charisiou[1,2], A. Baklavaridis[1], V.G. Papadakis[2], M.A. Goula[1,*]

[1]Department of Environmental and Pollution Control Engineering, Technological Educational Institute of Western Macedonia (TEIWM), GR – 50100, Koila, Kozani, Greece
[2]Department of Environmental and Natural Resources Management, Patras University, Agrinio, Greece

ABSTRACT

As it is well known, fossil fuels' power generation emits large amounts of greenhouse gases which affect the planet's climate in adverse ways. The energetic utilization of biogas, a gas mixture consisting mainly of CH_4 and CO_2 via the reforming or the dry reforming of methane reaction (DRM) is of enormous interest as it converts to convert these two greenhouse gases into synthesis gas (H_2/CO mixtures). DRM can be integrated in the well-established downstream syngas chemistry leading to synthetic fuels like alcohols or hydrocarbons. Reforming with CO_2, rather than steam reforming (SRM) with H_2O yields syngas with lower H_2/CO ratios, that is especially attractive for oxo synthesis (hydroformylation) of aldehydes from alkenes and possibly also for Fischer–Tropsch synthesis of long chain hydrocarbons.

Nickel based catalysts have been extensively studied for both reactions, as they are highly active, but they suffer from fast deactivation by coking that can even lead to reactor blocking. It is thus desirable to learn more about their coking behavior, and their structural and catalytic stability. Until now, several attempts have been made to suppress coke formation on Ni catalysts using different supports. The addition of basic promoters such as CaO or MgO to Ni/Al_2O_3 catalysts can increase the activity and reduce carbon formation. The Lewis basicity of this kind of promoters enhances the chemisorption of CO_2, a characteristic that is proposed to reduce the Boudouard reaction by shifting the equilibrium toward CO. The formation of a $NiAl_2O_4$ spinel was found to have a suppressing effect on the carbon formation, while the reduction of $NiAl_2O_4$ compared to NiO results in smaller Ni crystallites.

In this work, un-promoted and promoted with 6.0 wt% MgO or CaO alumina supported nickel catalysts (8.0 wt% Ni) were studied for the biogas reforming reaction, in order to investigate the effect of the reaction temperature on (i) methane and carbon dioxide conversion, (ii) hydrogen yield, (iii) H_2/CO molar ratio of the produced gas mixtures at the outlet of the reactor. Supported nickel catalysts were synthesized following the wet impregnation method. The as synthesized Ni/Al_2O_3, Ni/MgO-Al_2O_3, Ni/CaO-Al_2O_3 samples were characterized by various techniques as the X-ray diffraction (XRD), Scanning Electron Microscope (SEM) and N_2 absorption/desorption isotherms (BET). Their chemical composition was determined using the Inductively Coupled Plasma Emission Spectrometry (ICP). Catalytic testing experiments were performed in a fixed-bed reactor at temperatures ranging from 500 to 850^{o}C and a feed gas mixture with a molar CH_4/CO_2 ratio of 1.5 simulating an ideal model biogas.

It was concluded that the Ni/MgO-Al_2O_3 and Ni/CaO-Al_2O_3 catalysts exhibit higher values for methane conversion (X_{CH4}), carbon dioxide conversion (X_{CO2}), hydrogen yield (Y_{H2}) compared to the ones of the Ni/Al catalyst for temperature ranging between 550 to 750^{o}C, while the opposite is evidenced for T>750^{o}C. It was also evidenced that the presence of magnesium or calcium oxide in the support ensures a quite stable H_2/CO molar ratio approaching to unity (ideal for the produced syngas) even for low reaction temperatures.

Keywords: biogas, synthesis gas, dry reforming, supported nickel catalysts

1. INTRODUCTION

As is well documented, the unprecedented development that the world has experienced since the industrial revolution has been based upon its insatiable appetite for energy. In the words of the late economist E.F. Schumacher energy is *"not just another commodity, but the precondition of all commodities, a basic factor equal with air, water, and earth"* (Sovacool and Mukherjee, 2011). Recent statistical data from the World Energy Council (2013) show that 82% of the total commercial energy consumed in the world was derived from fossil sources (Figure 1). The figure was even higher in the transport sector, standing at 98%.

Serious concerns about the future availability of those non-renewable fuels are increasingly prominent in public awareness and discourse. For a number of years the focus has mainly fallen upon crude oil, with clear divisions amongst researchers who predict a near future peak in oil production (e.g. Aleklett and Campbell, 2003; Almeida and Silva, 2009; Bentley, 2002; Campbell and Laherrere, 1998; Jakobsson et al., 2012) and those that see no availability problems in the foreseeable future (e.g. Jackson, 2006; Maugeri, 2004; Odell, 2010; Radetzki, 2010). Peak gas and peak coal production have also been investigated (Laherrere, 2003; Simmons, 2007). What is beyond doubt however is the finite nature of these resources, which ultimately means that their extraction per unit of time has an upper limit after which it starts declining until the final depletion of stock.

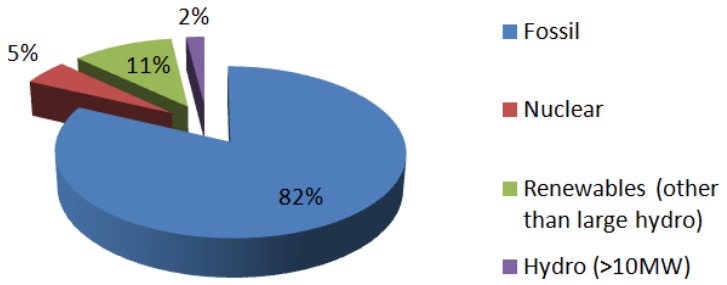

Figure 1. Total primary energy supply in 2011 by resource (World Energy Council, 2013)

The anxiety that surrounds the availability of fossil resources is compounded by issues relating to accessibility and affordability, a common theme in energy security discussions (Winzer, 2012). There is agreement that the continuity of supply is subject to a multitude of risks that can be broadly divided into two categories: technical risk sources and human risk sources (Gnansounou, 2008; Rutherford et al., 2007). The former include failure of infrastructure components such as transmission lines, while the latter concern events such as, strategic withholding of supplies, terrorism and geopolitical risks.

Other potential threats to the future sustainability of global energy markets include both the weak regulatory institutions and political accountability, and the outright political instability that characterizes many producer countries (Al-Kasim et al., 2013; Ross, 2001), the emergence of new consumers such as China and India (Sahira and Qureshi, 2007; Zhang, 2011), the phenomenon of recourse nationalism (Stegen, 2011), and the discrepancy in reserve holding between National Oil Companies (NOCs), also known as state-owned energy champions, and International Oil Companies (IOCs) (Winzer, 2012).

The effects that the issues highlighted above can have on 'global well being' become terrifying when one adds to the equation the issue of 'climate change'. The rapid increase in anthropogenic greenhouse gas concentrations in the last several decades has caused observable changes in global climate on all continents. Carbon dioxide, the primary causative agent of climate change has increased from a long-term mean average of 275 ppm in the pre-

industrial age to the current level of 400 ppm (Mathews, 2014). If there is no concerted action by the global community, CO_2 levels could increase by 130% by mid century resulting in large-scale climate changes such as the disintegration of the West Antarctic ice sheet and subsequent sea level rises, large-scale coral reef bleaching, and shutdown of the ocean circulation system (van der Pol, et. al., 2015; Wiréhn, et. al., 2015).

The global strategy to reduce dependence on fossil resources is based on reducing energy consumption, by applying energy savings programs focused on energy demand reduction and energy efficiency in the transportation, industrial and domestic sectors, and by developing and promoting Renewable Energy Systems (RESs), which include wind power, photovoltaic (PV) cells, concentrating solar power (CSP), hydroelectric plants and biomass/ bioenergy (Charisiou, Goula, 2014).

In addition to the energy related issues briefly touched upon above, the population growth that the earth has experienced in the last 50 years has resulted in increased rates of waste generation and the improper handling of wastes, created in turn a host of environmental issues (Noor, et al., 2013). Usman et al., (2015) has reported that there are about 3 billion urban residents generating 1.2 kg per person per day (1.3 billion tons per year) and it is estimated that in 2025 this figure will likely rise to 4.3 billion residents generating 1.42 kg per person per day, (meaning o production of 2.2 billion tons of waste per year). Moreover, for developed countries, the rate of the increase was estimated to be 3.2–4.5% and for developing nations around 2–3% (Abushammala, et al., 2011).

2. BIOGAS PRODUCTION AND UTILIZATION

Biomass encompasses among others, vegetation, energy crops, as well as biosolids, animal, forestry and agricultural residues, the organic fraction of municipal waste and certain types of industrial wastes. Its appeal is due to its potential worldwide availability, its conversion efficiency and its ability to be produced and consumed on a CO_2-neutral basis. The production of second-generation biofuels obtained by waste biomass is actively supported globally to avoid the direct and side effects that stem from the energetic utilization of energy crops (Iakovou, et. Al. 2010), and further support effectively waste management policies.

Biogas refers broadly to a gas produced by anaerobic digestion or fermentation of any biodegradable organic matter, including municipal solid waste, sewage sludge, agricultural wastes, animal dung, and energy crops. The main components of biogas are methane (55-75%) and carbon dioxide (24-44%), which are the principal greenhouse gases (Chattanathan, et al., 2014). It is worth noting that methane has approximately 21 times the greenhouse gas effect of CO_2. The use of biogas presents a number of advantages in comparison to other RES as: (a) its chemical energy can be converted into mechanical energy by controlled combustion processes in stationary engines, which then put in motion the generators to promote a direct conversion into electrical energy, (b) it can be used to co-generate thermal energy, generating hot water and steam with the engine's high temperatures, (c) it can be burned to generate heat energy in boilers, and (d) it can be applied as fuel to automotive and stationary engines (Alves, et. al., 2013; Bereketidou and Goula, 2012; Damrongsak and Tippayawong, 2010; Solomon and Lora, 2009).

In most countries where the development of this resource has taken place, biogas is predominantly used for Combined Heat and Power (CHP) applications, in electricity generation and as feed-in to the national grid (Poeschl et al., 2010). Usually, importance is attached to the recovery and utilization of Landfill Gas (LFG, with approximately 85% and 75% of all biogas output in Britain and the United States respectively), while most digester projects are located on dairy farms. However, a large degree of geographical variability in biogas utilization and

development exists (Figure 2), with the EU and in particular Germany) being the world leader in the deployment of biogas technology (Deng et al., 2014).

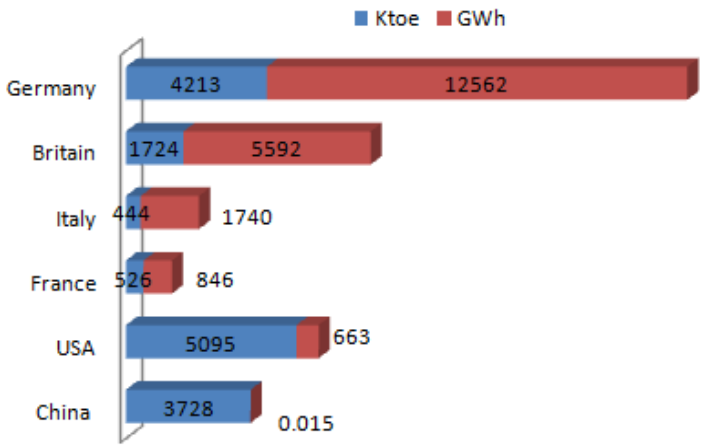

Figure 2. Biogas yield (Ktoe) and biogas power generation (GWh)

Although there are various types of applications, new biogas alternatives need to be strategically exploited to consolidate its power generation potential and significance. For this reason extensive research is being performed to convert methane into liquid fuels or higher hydrocarbons. Researchers have investigated the production of methanol, formaldehyde, propanol, benzene and other aromatics by direct oxidative conversion of methane. Unfortunately, all the aforementioned processes have low yields or are unfeasible on an industrial-scale (Li, et al., 2011). Various technologies are available to produce synthesis gas (syn-gas) which is a building block for valuable liquid fuels and chemicals such as FischerTropsch oil, methanol and dimethyl ether (Bereketidou and Goula, 2012). The three processes that have drawn industrial attention are: (i) steam reforming of methane (R-1), (ii) partial oxidation of methane with oxygen or air (R-2), and (iii) dry reforming of methane with carbon dioxide (R-3).

Steam reforming, SR: $CH_4 + H_2O \rightarrow CO + 3H_2 \quad (\Delta H = 222.4\ kJ/mol)$ (R1)

Partial oxidation, PO: $CH_4 + \frac{1}{2}O_2 \rightarrow CO + 2H_2 \quad (\Delta H = -22.6\ kJ/mol)$ (R2)

Dry reforming, DR: $CH_4 + CO_2 \rightarrow 2CO + 2H_2 \quad (\Delta H = 247.3\ kJ/mol)$ (R3)

The first two processes are well established and have a number of advantages and disadvantages. The steam reforming of methane produces a higher ratio of syn-gas (H_2/CO = 3) compared to that required for Fischer Tropsch or methanol synthesis (H_2/CO = 2) (Usman et al., 2015). However, the process is energy intensive due to its endothermic nature and requires high investments of capital (Nieva, et al., 2014). Moreover, a higher H_2O/CH_4 ratio is required to produce higher yields of hydrogen, which makes steam reforming of methane energetically unfavorable leading to the deactivation of the catalyst. In addition, steam reforming faces corrosion issues and requires a desulphurization unit (Carvalho, et al., 2009). Partial oxidation of methane is suitable for the production of heavier hydrocarbons and naphtha. The advantages of this process are high conversion rates, high selectivity and very short residence time, but the

exothermic nature of the reaction induces hot spots on the catalysts used and makes the operation difficult to control (Larimi and Alavi, 2012). In comparison, the dry reforming of methane yields lower syn-gas ratios (H_2/CO=1), which is suitable for the synthesis of oxygenated chemicals and hydrocarbons from FischerTropsch synthesis (Bereketidou and Goula, 2012).

2.1 Biogas dry reforming reaction

DRM (R-1) is a highly endothermic reaction that takes place catalytically in a temperature range between 600-800 °C, producing a syngas with a theoretical H_2:CO molar ratio of 1:1. Side reactions like water gas shift (R-2), methanation (R-3), carbon formation (R-4), carbon monoxide disproportionation (Boudouard reaction (R-5), gasification reaction (R-6), and oxidation reactions (R-7, R-8) can take place on the catalyst surface, affecting the performance of the above mentioned processes. Shown in Figure 3 is an illustration of the overall process of CH_4 and CO_2 being converted to CO and H_2 on a supported metal catalyst.

Water gas shift (WGS): $n\left(CO + H_2O \rightleftharpoons CO_2 + H_2\right) \quad \left(\Delta H = -41.0\ kJ/mol\right)$ (R4)

Methanation (MTH): $n\left(CO + 3H_2 \rightleftharpoons CH_4 + H_2O\right) \quad \left(\Delta H = -208.2\ kJ/mol\right)$ (R5)

Decomposition (D): $C_nH_mO_k \rightarrow \left(n-k\right)C + \left(\frac{m}{2}\right)H_2 + kCO$ (R6)

Boudouard (Boud): $2CO \rightleftharpoons CO_2 + C \quad \left(\Delta H = -171.5\ kJ/mol\right)$ (R7)

Coke gasification (GS): $C + H_2O \rightleftharpoons CO + H_2 \quad \left(\Delta H = 139.0\ kJ/mol\right)$ (R8)

Coke oxidation (CO): $C + \frac{1}{2}O_2 \rightarrow CO \quad \left(\Delta H = -110.5\ kJ/mol\right)$ (R9)

Coke oxidation (CO): $C + O_2 \rightarrow CO_2 \quad \left(\Delta H = -395.6\ kJ/mol\right)$ (R10)

2.2 Influence of active metal and of supports on catalytic activity

The dry reforming of methane has been investigated with noble (Rh, Ru, Pd and Pt) and non-noble metal (Ni, Co and Fe) based catalysts (Liu, et al., 2009). Noble metal catalysts have drawn attention for their superior coking resistance, higher stability and activity especially for higher temperature applications (>750 ^oC) (Usman et al., 2015). However, noble metals cannot be applied on an industrial scale due to their high cost. In that respect Ni appears to be the most suitable choice for both technical and economic reasons (Courson, et al., 2000). It has been also demonstrated that if a strong nickel–support interaction exists initially in the catalyst, nickel sintering as well as carbon deposition can be avoided (Hayakawa, et al., 1997; Provendier, et al., 1999). Furthermore, supports play an important role in catalytic activity due to their probable chemical effect, besides their interaction with the active phase. It is also known that supports with large surface area and usually small or medium pores, such as alumina, normally exhibit additional mass transfer limitation issues of the reactant (Tao, et al., 2010).

In general, Nickel-based on alumina catalysts are reported to be deactivated due to their coking and sintering problems. Moreover, although alumina has been commonly used as the supporting material, the nickel spinel phase ($NiAl_2O_4$) formed on its surface seems to influence

the whole process (Goula, et al., 1996; Juan-Juan, et al., 2009; Sahli, et al., 2006; Xu, et al., 2009). In order to improve the catalytic performance of the nickel/alumina catalysts, several parameters are modified, such as the improving characteristics of the support by introducing structural or surface promoters, or differentiating the active metal loading and the catalyst's preparation technique (Aghamohammadi, et al., 2013; Bereketidou and Goula, 2012; Dias and Assaf, 2003; Fan, et al., 2011; Garcıa, et al., 2009; Roh and Jun, 2008). Choudhary, et al., (1995) reported that the catalyst precoated with MgO and CaO showed high activity compared to that of catalyst without precoating. Koo, et al. (2008) reported that the MgO promoted Ni/Al_2O_3 catalyst forms $MgAl_2O_4$ spinel phase, which is stable at high temperature and effectively prevents coke formation by increasing the CO_2 adsorption due to the increase in base strength on the surface of catalyst. The addition, calcium led to positive catalytic effect in terms of higher activity and coking resistance (Ranjbar, et al., 2012). Optimized Ca loading was found to play a critical role in coke removal, through its effect on Ni particle size, valence band of catalyst and steam gasification of coke (Choong, et al., 2011).

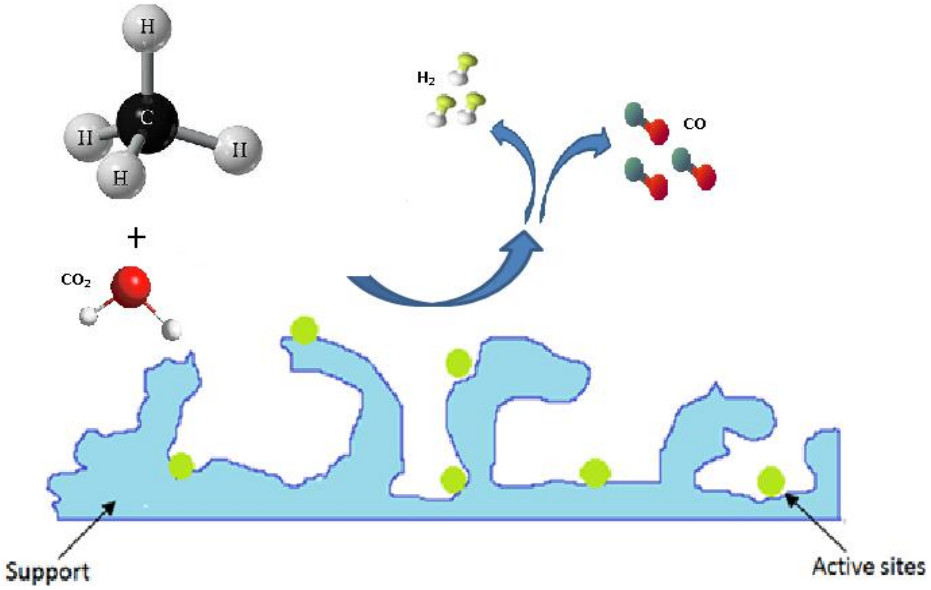

Figure 3. Illustration showing the overall process of CH_4 and CO_2 being converted to CO and H_2 on a supported metal catalyst

3. MATERIALS AND METHODS

3.1 Catalysts preparation

The calcium-alumina and magnesium-alumina supports were obtained by impregnating the γ-alumina (Akzo, 350 – 500 μm, S_{BET} = 195 m^2g^{-1}) with an aqueous solution of $Ca(NO_3)_2$ $6H_2O$ and $Mg(NO_3)_2$ $4H_2O$ with appropriate concentration at room temperature. The physicochemical properties of the γ-alumina used in this study are presented in Table 1. Supported nickel catalysts were prepared following the wet impregnation method and by using $Ni(NO_3)_2$ $6H_2O$ aqueous solutions with the proper concentration, in order to obtain a final catalyst with Ni content of about 8 wt%. All the catalyst samples were evaporated by using a rotary evaporator at 75 ^oC for 5 hr and dried at 120 ^oC for 12 hr followed by calcination at 800 ^oC for 4 hr. The samples were labeled as Ni/Al, Ni/CaAl and Ni/MgAl.

Table 1. Physicochemical properties of the γ-alumina used in the study

Property	Value
Mean pore diameter (α)	7.8×10^{-9} m
Surface area (S_{BET})	281 $m^2 g^{-1}$
Bed density (ρ_B)	5.7×10^5 g m^{-3}
Pore volume (V_p)	0.65 ml g^{-1}
Average diameter (d)	350-500 μm

3.2 Catalysts characterization

Surface areas (S_{BET}) of the catalytic samples were determined by the N_2 adsorption-desorption isotherms at -196^{o}C using the Nova 2200e (Quantachrome) flow apparatus, according to Brunauer-Emmett-Teller (BET) method at the relative pressure in the range of 0.05–0.30. The total pore volume calculation was based on nitrogen volume at the highest relative pressure, whereas the average pore size diameter was determined by the Barrett-Joyner-Halenda (BJH) method. Prior to the measurements the samples were degassed at 350^{o}C for 5 h under vacuum.

The total metal loading (wt%) of the final catalysts was determined by Inductively Coupled Plasma Atomic Emission Spectroscopy (ICP-AES) on a Perkin-Elmer Optima 4300DV apparatus. The wavelengths selected were at 341.476, 227.022, and 231.604 nm. The selected conditions of the measurement were: (i) Plasma flow: 15 L/min, (ii) Auxiliary flow: 0.2 L/min, (iii) Nebulize flow: 0.6 L/min, (iv) RF Power: 1300 watts, (v) Plasma View: radial view, and (vi) Sample Flow Rate: 2 mL/min. The acid digestion procedure involved the weighting of each sample to the nearest 0.00001^{o}g in a Teflon beaker and its transportation to a fume hood, where 1 ml of concentrated sulphuric acid was added. The mixture was then heated to dryness at low heat on a hot plate overnight. Afterwards, 2 ml of concentrated hydrochloric acid and 2 ml of concentrated nitric acid were added to the beaker with the heating being terminated after 5-10 min, when the reaction of dissolution was completed. At this point, about 2 ml of de-ionized water were added and the beaker was left to cool. The resulting clear solution was loaded carefully in a 50 ml volumetric flask in order to make up an accurate fixed volume adding de-ionized water. Each sample was measured thrice, in order to check repeatability.

The catalysts' crystalline structure was determined by applying the X-ray diffraction (XRD) technique, using a ThermoAl diffractometer at 40 kV and 30 mA with Cu K_α radiation (λ=1.54178 nm). Diffractograms were recorded in the 2θ=2-70^o range at a scanning rate of 0.04^o over 1.2 min^{-1}. The diffraction pattern was identified by comparison with those of known structure in the JCPDS (Joint Committee of Powder Diffraction Standards) database. It should be noted that the XRD technique was used for both fresh and reduced samples.

Morphological examination of both fresh and used catalysts was done using Scanning Electron Microscopy (SEM) in a JEOL 6610LV. The elemental analysis, by means of Energy Dispersive Spectroscopy (EDS), was carried out using a large area (80mm^2) silicon drift detector (X-Max 80 Oxford Instruments). Images, elements maps and spectra were acquired and analyzed with the AZtech Nanoanalysis software (Oxford Instruments).

3.3 Catalytic performance measurements

The biogas reforming reaction was carried out at atmospheric pressure, in a fixed-bed reactor (Figure 4) at temperatures ranging from 500 to 850^{o}C. The total flow rate used was 100 ml min^{-1}, consisting of a gas mixture of CH_4/CO_2/He (30% v/v, 20% v/v and 50% v/v respectively), corresponding to a Weight Hourly Space Velocity (WHSV) of 120,000 mL g^{-1} h^{-1}. Thus, the feed gas mixture had a constant molar CH_4/CO_2 ratio of 1.5 simulating an ideal model biogas (Bereketidou & Goula, 2012). The amount of catalyst used in the catalytic bed was 50 mg. The reaction temperature was controlled by a thermocouple placed in the middle of the catalytic bed.

The gaseous reaction products were analyzed on-line by gas chromatography in a CG-Agilent 7890A gas chromatographer with two columns in parallel, HP-Plot-Q (19095-Q04, 30 m length, 0.530 mm I.D.) and HP-Molesieve (19095P-MSO, 30 m length, 0.530 mm I.D.), equipped with a TCD and FID detectors. Prior to performing any catalytic reaction measurement, catalysts were in situ activated by flowing pure hydrogen for 2 hours at 800°C.

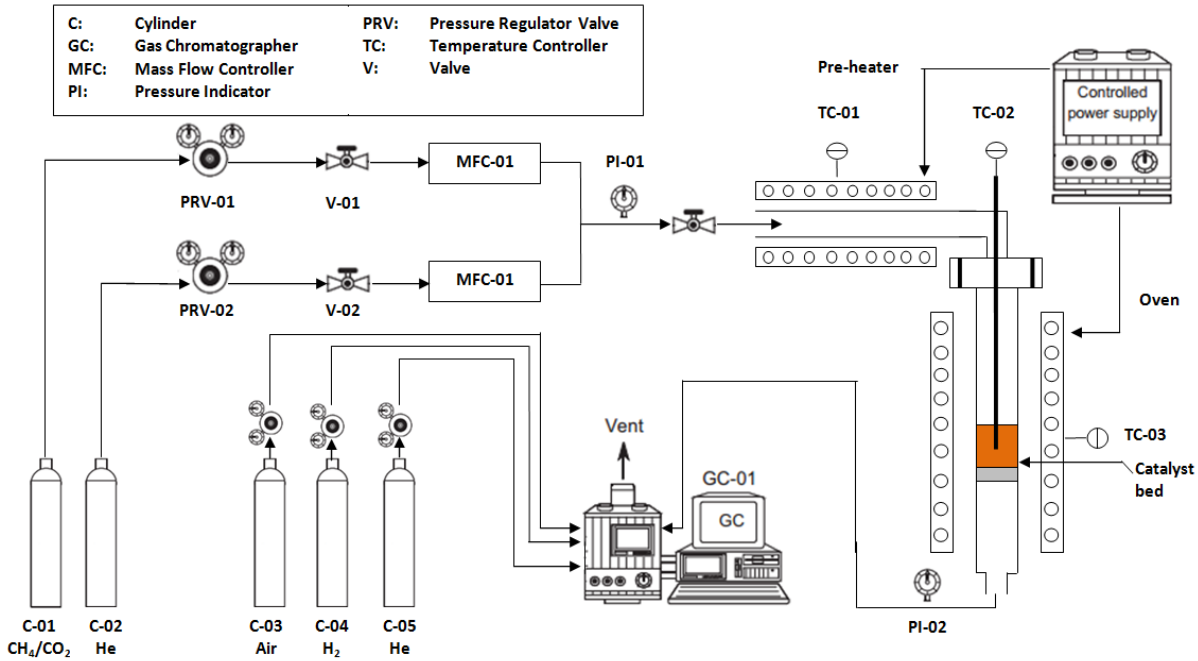

Figure 4. Schematic flow chart of experimental setup for activity test of catalysts towards biogas dry reforming

3.4 Reaction metrics

According to the analysis and metering system mentioned above, the conversion of CO_2 and CH_4 can be calculated as defined in Eqs. (1) and (2). Moreover, the selectivity of H_2, the yield of H_2 and the yield of CO can be calculated as defined in Eqs. (3)–(5), respectively:

$$X_{CH_4}(\%) = \frac{F_{CH_4,in} - F_{CH_4,out}}{F_{CH_4,in}} \times 100 \qquad (1)$$

$$X_{CO_2}(\%) = \frac{F_{CO_2,in} - F_{CO_2,out}}{F_{CO_2,in}} \times 100 \qquad (2)$$

$$S_{H_2}(\%) = \frac{F_{H_2}}{2\left(F_{CH_4,in} - F_{CH_4,out}\right)} \times 100 \qquad (3)$$

$$Y_{H_2}(\%) = \frac{F_{H_2}}{2F_{CH_4,in}} \times 100 \qquad (4)$$

$$Y_{CO}(\%) = \frac{F_{CO}}{F_{CH_4,in} + F_{CO_2,in}} \times 100 \qquad (5)$$

where *Fi,in* or *Fi,out* is the flow rate of each component in feed or effluent.

4. RESULTS AND DISCUSSION

4.1 Characterisation results

In Table 2 the physicochemical properties of all samples are presented. As can be observed, calcination to 800 ^{o}C has significantly decreased the specific surface area (SSA, i.e., S_{BET}) of the Al_2O_3 support from 281 m^2g^{-1} to 195 m^2g^{-1}. Further reduction of the SSA occurred with the introduction of Ni on the supporting material, whereas the pore volume (Vp) was not significantly altered. The lower surface area can be attributed to the fact that the internal surface area of the support pore system is probably progressively covered by nickel species adsorbed on alumina active sites forming a layer (Cheng, et al., 2011). The same reduction is observed with the introduction of MgO and CaO on the alumina support. Although measurements are not available, the SSA of the Ni/MgO and Ni/CaO catalysts would have been further reduced with the introduction of Ni on the supports. The ICP results (metal loading) show that 7.14 wt% of nickel was achieved for the Ni/Al catalyst, while the Ni/MgO and Ni/CaO catalysts have comparable promoter levels (5.68 wt% of Mg and 6.37 wt% of Ca).

Table 2: Characterization results of the calcined and reduced catalysts

Catalyst	S_{BET} (m^2g^{-1})	V_p (ml g^{-1})	Metal loading (wt%)
Al (un)	281		
Al (c)	195	0.65	-
MgO-Al (c)	186	0.59	5.68 (Mg)
CaO-Al (c)	181	0.57	6.37 (Ca)
Ni/Al (c)	158	0.57	7.14 (Ni)
Ni/Al (r)	-	-	-
Ni/MgO-Al (c)	n/a	n/a	n/a
Ni/MgO-Al (r)	-	-	-
Ni/CaO-Al (c)	n/a	n/a	n/a
Ni/CaO-Al (r)	-	-	-

Note: un=untreated, c=calcinated, r=reduced

Figure 5 depicts the XRD patterns of the Ni/Al catalyst after calcination and after reduction. For the calcinated Ni/Al sample, characteristic peaks at 2θ=35.2^{o}, 47.2^{o} and 67.6^{o} assigned to γ-Al_2O_3 can be observed. Moreover, no reflections belonging to transition aluminas, θ-alumina (2θ=25.6^{o} and 43.3^{o}) or alpha-alumina (2θ=31.2^{o} and 36.6^{o}) were observed, indicating that no alumina transformation was realized at the calcination temperature used for the catalysts preparation (T=800^{o}C). Peaks of the spinel nickel aluminate phase ($NiAl_2O_4$), indicated by the intensity of diffraction lines at 2θ=19.0^{o}, 32.0^{o}, 37.0^{o}, 45.0^{o}, 60.2^{o} and 65.9^{o} were also detected. The formation of $NiAl_2O_4$ is caused by the reaction of NiO and Al_2O_3 due to the high calcination temperature (Dou, et al., 2014). Nickel aluminate crystallizes in the cubic system and belongs to Fd-3 m space group. Typically, the framework of the spinel structures consists of an ensemble

of tetrahedral and octahedral coordination occupied by bivalent (Ni^{2+}) and trivalent (Al^{3+}) cations, respectively. This distribution can change when the Ni^{2+} partially adopts the octahedral site while the tetrahedral site hosts the Al^{3+} together with Ni^{2+} ions. This structural flexibility generates a family of compounds of inverse spinel structure described as $Ni_{1-x}[Ni_xAl_{2-x}]O_4$ (0<x<1) (Boukha, et al., 2014; Jiménez-González, et. al., 2014). At the same time the nickel oxide structure was not detected (expected at 2θ=43.5° and 63.1°), indicating that if these species were present, they would be quite small, since XRD can typically only detect crystalline phases that are larger than several nm. Thus, it is possible that NiO exists on these catalysts, but with crystallite sizes smaller than the XRD detection limit or that their structure is nearly amorphous (Bobadilla, et al., 2015; Melchor-Hernández, et al., 2013). The main differences between the XRD patterns of the calcined and reduced Ni/Al catalyst, are the decreasing intensities of Al_2O_3 and $NiAl_2O_4$ peaks and the appearance of small peaks due to the presence of metallic Ni^o at 2θ=44.0^o and 51.2^o. The low intensity of these peaks can be related to the size of the metallic nickel species (Franchini, et al., 2014). Thus, the reduction at 800^{o}C didn't reduce the entire $NiAl_2O_4$ phase (it just slightly decreased the intensity of the nickel aluminate's peaks), and it can be assumed that a surface $NiAl_2O_4$ spinel coexisted with the γ-Al_2O_3 support.

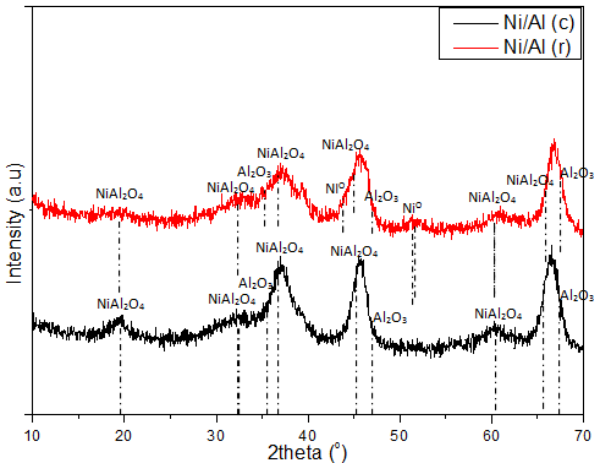

Figure 5. XRD patterns of calcined and reduced Ni/Al catalysts

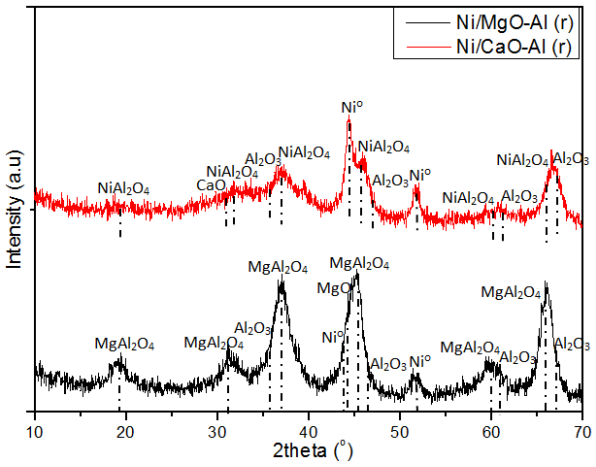

Figure 6. XRD patterns of the reduced Ni/MgO-Al and Ni/CaO-Al catalysts

Table 3. Crystalline phases of supports and catalysts

Sample	Crystalline phases
Al (c)	Al_2O_3
MgO-Al (c)	MgO, Al_2O_3
CaO-Al (c)	CaO, Al_2O_3
Ni/Al (c)	NiA_2O_4, Al_2O_3
Ni/Al (r)	NiA_2O_4, Ni^o, Al_2O_3
Ni/MgO-Al (r)	MgO, $MgAl_2O_4$, Ni^o, Al_2O_3
Ni/CaO-Al (r)	CaO, $NiAl_2O_4$, Ni^o, Al_2O_3

Note: c=calcinated, r=reduced

Figure 6 depicts the XRD patterns of the reduced Ni/MgO-Al and Ni/CaO-Al catalysts. For the Ni/MgO-Al sample, characteristic peaks at 2θ= 35.7^o, 38.6^o, 46.9^o, 62.1^o, and 67.3^o

corresponding to γ-Al_2O_3 can be observed. MgO appears at the diffraction line 2θ= 44.7°, while peaks of the spinel magnesium aluminate phase ($MgAl_2O_4$) at 2θ= 19.2°, 31.5°, 37.1°, 45.3°, 60.0°, and 66.1°. For the Ni/CaO-Al sample, peaks assigned to the γ-alumina appear at 2θ= 37.9°, 46.6°, 61.6°, 66.8°, and 68.5°, CaO at 2θ= 31.0° and $NiAl_2O_4$ at 2θ= 19.1°, 31.4°, 37.0°, 45.0°, 60.0°, and 65.9°. The presence of metallic Ni° was observed for both catalysts at 2θ=44.4° and 51.5°. It is worth noting that the size of the peaks of metallic Ni° are Ni/Al<Ni/MgO-Al<Ni/CaO-Al. Table 3 summarizes the crystalline phases that were detected for both catalysts and supports.

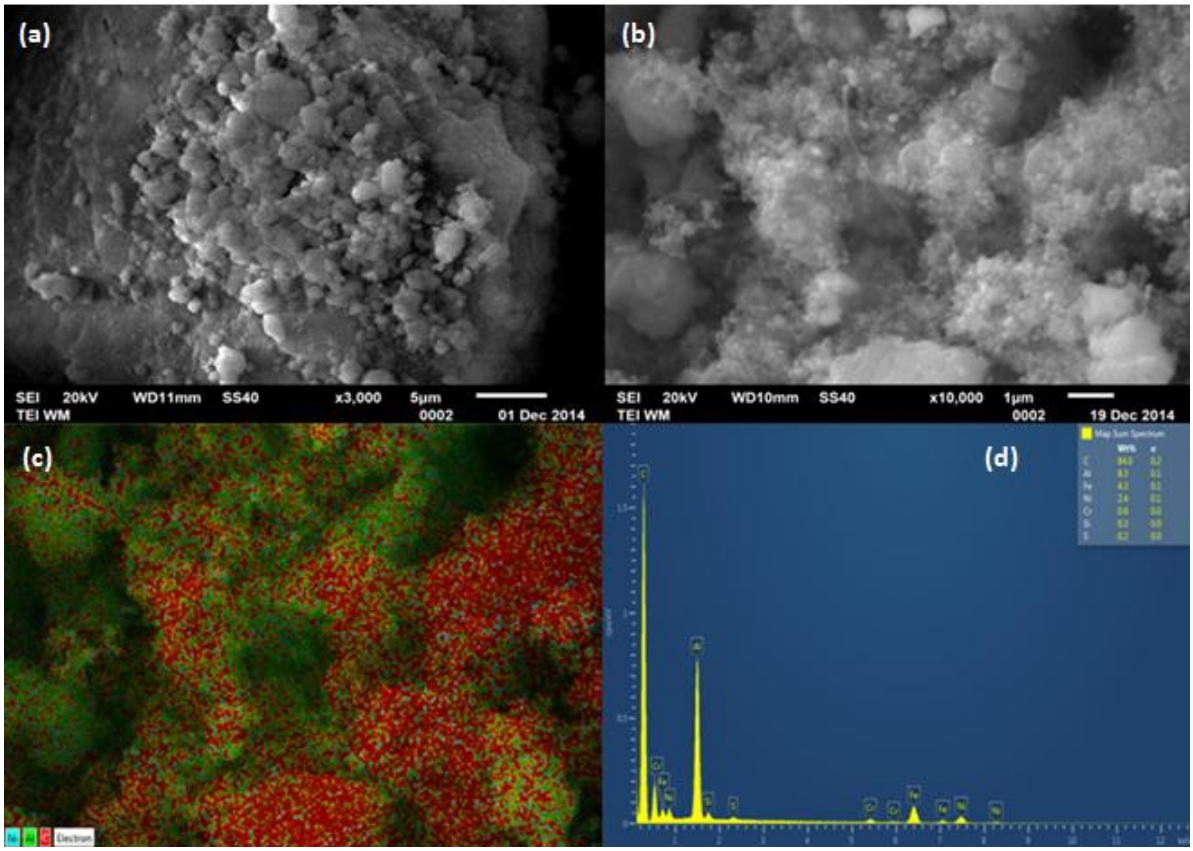

Figure 7. SEM images and mapping of fresh and used Ni/Al catalyst: (a) Fresh catalyst b) Used catalyst , c) Carbon mapping of used catalyst d) EDS spectra of used catalyst

SEM has been used for the examination of the catalysts surface texture and morphology. Figure 7a shows the SEM images of the Ni/Al catalyst before use (fresh). As can be observed the catalyst is of non uniform morphology and includes large ensembles, as well as, micro and nano particles. The nano particles can be assumed to be NiO and/or Ni°, while the larger particles can be presumed to be alumina (Dou, et al., 2014). As can be observed from Figure 7(b), after the dry reforming process, some of the catalyst particles have cracked and fragmented into smaller particles. In addition, carbon filaments are observed surrounding the catalyst surfaces and partially covering the surface of the reacted catalyst. It has been suggested that the Ni particles are sintered until a critical size that favors the formation of filamentous carbon, while no filaments will grow below a certain minimum filament diameter (Seung-hoon, et al., 2014; Zhai, et al., 2011). When carbon mapping is performed (Fig. 7c) it reveals that in the Ni/Al catalyst, carbon is concentrated on specific areas, most probably those where metallic Ni° is to be found. This was also confirmed in the EDS spectra which showed

that only 2.4 % of the nickel could be identified (Fig. 7d). Figure 8a and 8b show the SEM images of the Ni/CaO-Al catalyst before use (fresh) at different magnifications (x400 for image (a), and x3000 for image (b)). As can be observed this catalyst comprises of much smaller particles than the Ni/Al catalyst, at sizes that can be measured in nm, indicating a better dispersion of the NiO and Ni^o particles.

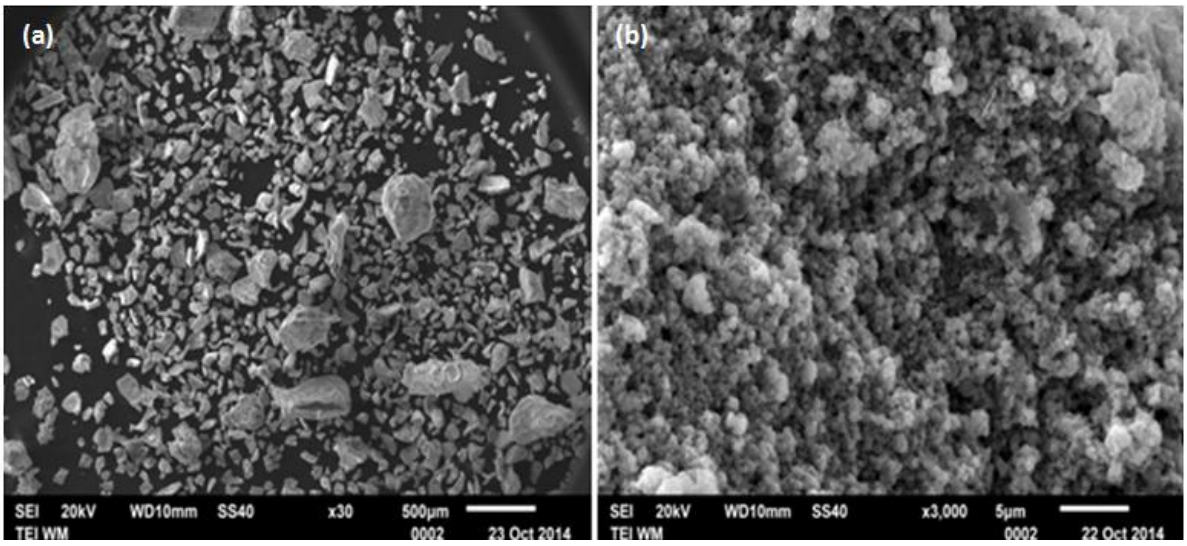

Figure 8. SEM images of fresh Ni/CaO-Al catalyst: (a) x30 magnification b) x3000 magnification

4.2. Catalyst activity and selectivity

In Figure 9 the influence of the reaction temperature to the methane (X_{CH4}) and carbon dioxide (X_{CO2}) conversion (Fig. 9a), to the hydrogen (Y_{H2}) yield (Fig. 9b) and to the molar ratio H_2/CO (Fig. 9c) is shown. It can be depicted that catalysts' activity, as well as hydrogen production increased with increasing temperature, which is in accordance with the strong endothermic character of the dry reforming reaction (Nikoo and Amin, 2011). It can be also observed that the Ni/CaO-Al and Ni/MgO-Al catalysts exhibit higher values for the X_{CH4} , X_{CO2} and Y_{H2} compared to the ones of the Ni/Al catalyst for temperature ranging between 550 to 750^{o}C, while the opposite is evidenced for T>750^{o}C. At CH_4/CO_2 ratio being equal to 1.5, CO_2 gas acts as a limiting reactant and is not able to convert CH_4 completely. Therefore, the high conversion of CH_4 at higher temperatures can be ascribed to the methane decomposition reaction ($CH_4 \leftrightarrow C + 2H_2$), as the predominant reaction to form hydrogen and carbon.

Moreover, according to thermodynamics, for CH_4/CO_2 ratios > 1, the amount of H_2 produced enhances within the investigated temperature, as CO_2 is the limiting reactant and the Reverse Water Gas Shift (RWGS) reaction cannot simultaneously improve along with the dry reforming reaction, as much as when the CH_4/CO_2 is lower than unit. As the RWGS is not being much involved, whenever CH_4/CO_2 ratio is lower, the DMR reaction proceeds better and faster suppressing the methane decomposition reaction, which causes the lower amount of H_2 production. On the other hand, higher temperatures favor CO production since all the reactions involved in CO production are endo-thermic. Higher experimental CO and H_2 yields than their equilibrium ones, along with high methane conversions, could provide evidence for significant ability of the catalyst in dissociation of CO_2 followed by CO and O production, as well as improving CO_2 reforming of methane.

As it can be observed in Figure 9c, the H_2/CO molar ratio increases with increasing temperature approaching the value of 1, for T = 850 ^{o}C for all the catalysts. It should also be

noticed that its value remains higher for the catalysts supported on modified with MgO or CaO alumina for the whole temperature range, revealing an improved catalytic performance. Specifically, for the Ni/MgO-Al catalyst, its value ranges between 0.8 to 1.0, for the Ni/CaO-Al 0.6 to 1.0 and for the Ni/Al 0.3 to 1.0, revealing that the presence of magnesium or calcium oxide in the support ensures a high and quite stable H_2/CO molar ratio (almost ideal for the produced syngas) even for low reaction temperatures. This is in accordance with other researchers' result (Abdollahifar, et al., 2014) who reported that the activity of a Ni/Al_2O_3–MgO nanocatalyst with Al/Mg ratio of 1.5, prepared by the sonochemistry method, could reach thermodynamic equilibrium conversions and H_2/CO ratios.

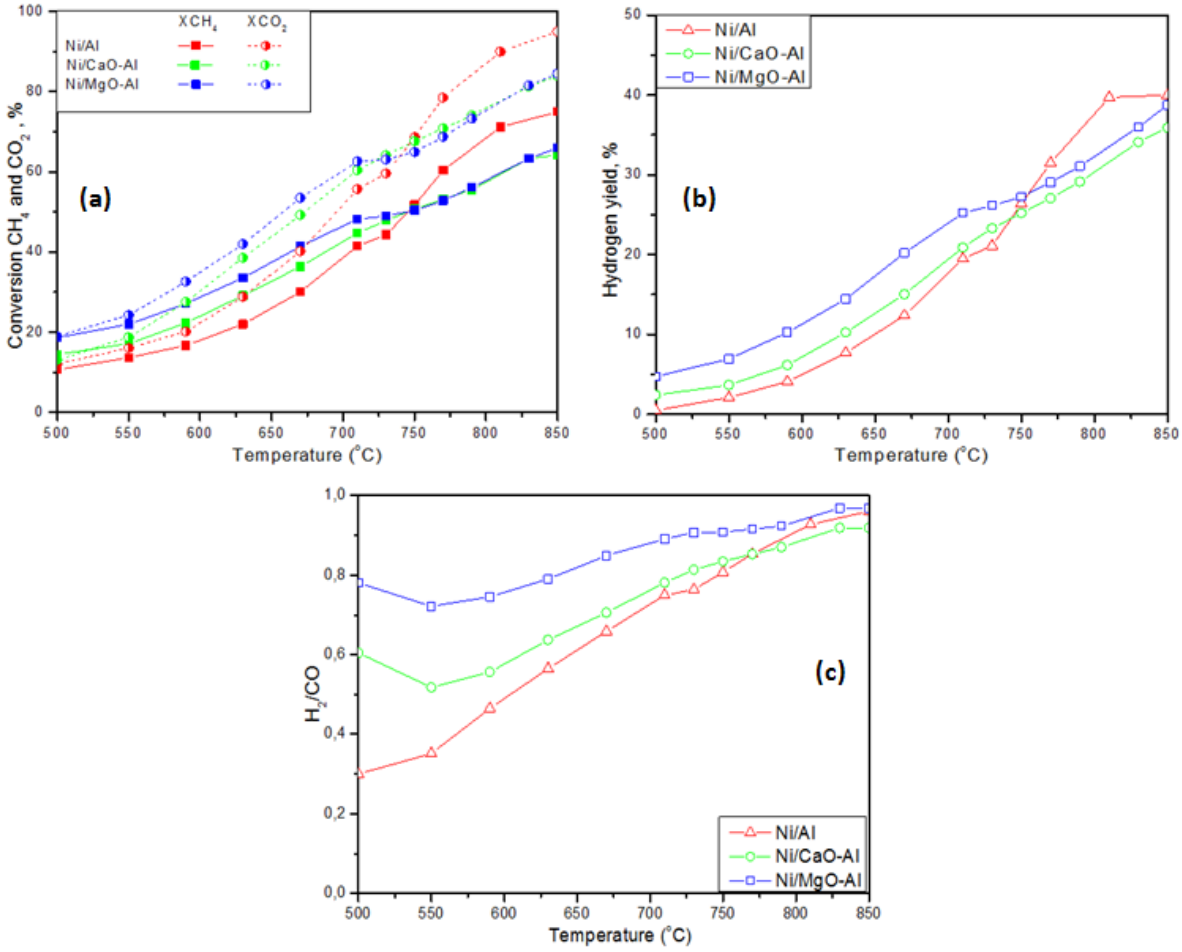

Figure 9. (a) Conversion of CH_4 and CO_2, (b) Hydrogen yield, (c) Molar ratio H_2/CO

The promotional effect of magnesium oxide to the catalytic activity and stability of the Ni/MgO-Al catalyst can be attributed to the basic nature of MgO, the intimate interaction between Ni and the support, and rapid decomposition/ dissociation of CH_4 and CO_2, which results in preventing coke formation. Moreover, with a capacity for oxygen storage, MgO can release oxygen to oxidize the carbon formed on the catalyst surface (Son, et al, 2014). It was also found (Mette, et al., 2014) that the redox dynamics of a Ni/MgO-Al catalyst and its strong structural and chemical consequences have only a moderate influence on the activity in DRM at 900◦C, but lead to a stable attenuation of carbon formation due to a lower fraction of graphitic carbon after DRM in a fixed-bed reactor.

On the other side, calcium is a metal with basic properties and has been tested as catalyst by several research groups in different kinds of reactions, such as dry reforming of methane, Fischer-Tropsch synthesis, propane dehydrogenation and hydro-desulfurization of petroleum feedstocks (Choong et al., 2011). Therefore it is known that CaO has high catalytic activity in different reactions and resistance to coking. Considering the structural changes, it was observed that the CaO addition favored the formation of nickel species in lower interaction with the support, thus requiring, a lower activation temperature (Elias et al., 2013).

Generally, it is believed that the addition of basic modifiers can be an efficient way for attenuating carbon formation during CRM reaction (Xu, et al., 2013). Particularly, the presence of the basic center will strengthen the chemisorption of CO_2 and promote the coke elimination reaction, considerably reducing the surface carbon deposition. Besides, incorporating the basic sites will largely reduce the concentration of Lewis acid centers, which will promise lower coke deriving from surface acid for CRM (Martinez, et al. 2004; Horiuchi, et al. 1998; Yang, et al. 2010). Therefore, the alkali metal oxides, alkaline earth metal oxides, and even rare earth metal oxides, such as K_2O, MgO, La_2O_3 , etc, are usually selected as basic modifiers or supports for nickel based catalysts (Rezaei, et al., 2008; Yang, et al., 2010; Hua, et al., 2010).

5. CONCLUSIONS

In this work, un-promoted and promoted with 6.0 wt% MgO or CaO alumina supported nickel catalysts (8.0 wt% Ni) were studied for the biogas reforming reaction, in order to investigate the effect of the reaction temperature on (i) methane and carbon dioxide conversion, (ii) hydrogen yield, (iii) H_2/CO molar ratio of the produced gas mixtures at the outlet of the reactor. Supported nickel catalysts were synthesized following the wet impregnation method. The as synthesized Ni/Al_2O_3, $Ni/MgO\text{-}Al_2O_3$, $Ni/CaO\text{-}Al_2O_3$ samples were characterized by various techniques as the X-ray diffraction (XRD), Scanning Electron Microscope (SEM) and N_2 absorption/desorption isotherms (BET). Their chemical composition was determined using the Inductively Coupled Plasma Emission Spectrometry (ICP). Catalytic testing experiments were performed in a fixed-bed reactor at temperatures ranging from 500 to 850^{o}C and a feed gas mixture with a molar CH_4/CO_2 ratio of 1.5 simulating an ideal model biogas.

It was concluded that the $Ni/MgO\text{-}Al_2O_3$ and $Ni/CaO\text{-}Al_2O_3$ catalysts exhibit higher values for methane conversion (X_{CH4}), carbon dioxide conversion (X_{CO2}), hydrogen yield (Y_{H2}) compared to the ones of the Ni/Al catalyst for temperature ranging between 550 to 750^{o}C, while the opposite is evidenced for T>750^{o}C. It was also evidenced that the presence of magnesium or calcium oxide in the support ensures a quite stable H_2/CO molar ratio approaching to unity (ideal for the produced syngas) even for low reaction temperatures.

REFERENCES

Abdollahifar, M., Haghighi, M., Babaluo, A.A., 2014. Syngas production via dry reforming of methane over Ni/Al_2O_3 –MgO nanocatalyst synthesized using ultrasound energy, Journal of Industrial and Engineering Chemistry, 20, 1845–1851.

Abushammala, M.F., Basri, N.E.A., Basri, H., El-Shafie, A.H., Kadhum, A.A.H. 2011. Regional landfills methane emission inventory in Malaysia. Waste Management Resources, 863-873.

Aghamohammadi, S., Haghighi, M., Karimipour, S., 2013. A comparative synthesis and physicochemical characterizations of Ni/Al_2O_3-MgO nanocatalyst via sequential impregnation and sol-gel methods used for CO_2 reforming of methane. Journal of Nanoscience and Nanotechnology, 13, 4872-4882.

Aleklett, K., Campbell, C.J., 2003. The peak and decline of world oil and gas production. Minerals & Energy 18, 5-20.

Al-Kasim, F., Soreide, T., Williams, A., 2013. Corruption and reduced oil production: An additional resource curse factor? Energy Policy 54, 137-147.

Almeida, P., Silva, P.D., 2009. The peak of oil production: Timings and market recognition. Energy Policy 37, 1267-1276.

Alves, H.J., Bley, C., Niklevicz, R.R., Frigo, E.P., Frigo, M.S., Coimbra-Araújo, C.H., 2013 Overview of hydrogen production technologies from biogas and the applications in fuel cells. International Journal of Hydrogen Energy 38(13), 5215–5225.

Bentley, R.W., 2002. Global oil & gas depletion: an overview. Energy Policy 30, 189-205.

Bereketidou, O.A., Goula, M.A., 2012. Biogas reforming for syngas production over nickel supported on ceria-alumina catalysts. Catalysis Today 195, 93-100.

Bobadilla, L.F., Penkova, A., Álvarez, A., Domínguez, M.I., Romero-Sarria, F., Centeno, M.A., Odriozola, J.A., 2015. Glycerol steam reforming on bimetallic NiSn/CeO_2–MgO–Al_2O_3 catalysts: Influence of the support, reaction parameters and deactivation/regeneration processes. Applied Catalysis A: General, 492, 38-47.

Boukha, Z., Jiménez-González, C., de Rivas, B., González-Velasco, J.R., Gutiérrez-Ortiz, J.I., López-Fonseca, R., 2014. Synthesis, characterisation and performance evaluation of spinel-derived Ni/Al2O3catalysts for various methane reforming reactions. Applied Catalysis B: Environmental, 158-159, 190-201.

Campbell, C.J., Laherrere, J.H., 1998. The end of cheap oil. Scientific American 278, 78-83.

Carvalho, L.S., Martins, A.R., Reyes, P., Oportus, M., Albonoz, A., Vicentini, V., Rangel, M.C., 2009. Preparation and characterization of Ru/MgO-Al_2O_3 catalysts for methane steam reforming. Catalysis Today, 142, 52-60.

Charisiou, N.D., Goula, M.A., 2014. Attitudes of Greek university students towards energy and the environment. Global Nest Journal 16(5) 856-865.

Chattanathan, S.A., Sdhikari, A., McVey, M., Fasina, O., 2014. Hydrogen production from biogas reforming and the effect of H_2S on CH_4 conversion. International Journal of Hydrogen Energy 39(35), 19905–19911.

Cheng, C.K. Foo, S.Y., Adesina, A.A., 2011. Steam reforming of glycerol over Ni/Al_2O_3 catalyst. Catalysis Today, 178, 25-33.

Choong, C.K.S., Zhong, Z., Huang, L., Wang, Z., Peng Ang, T., Borgna, A., Lin, J., Hong, L., Chen, L., 2011. Effect of calcium addition on catalytic ethanol steam reforming of Ni/Al_2O_3 : I. Catalytic stability, electronic properties and coking mechanism. Applied Catalysis A: General, 407, 145–154.

Choudhary, V.R., Uphade, B.S., Mamman, A.S., 1995. Large enhancement in methane-to-syngas conversion activity of supported Ni catalysts due to precoating of catalyst supports with MgO, CaO or rare-earth oxide. Catalysis Letters, 32, 387-390.

Courson, C., Makaga, E., Petit, C., Kiennemann, A. 2000. Development of Ni catalysts for gas production from biomass gasification. Reactivity in steam- and dry-reforming. Catalysis Today 63, 427–437.

Damrongsak, D., Tippayawong, N., 2010. Experimental investigation of an automotive air-conditioning system driven by a small biogas engine. Applied Thermal Engineering 30, 400–405.

Deng, Y., Xu, J., Liu, Y., Mancl, K., 2014. Biogas as a sustainable energy source in China: Regional development strategy application and decision making. Renewable and Sustainable Energy Reviews, 35, 294-303.

Dias, J.A.C., Assaf, J.M., 2003. Influence of calcium content in Ni/CaO/g-Al_2O_3 catalysts for CO_2-reforming of methane. Catalysis Today, 85, 59-68.

Dou, B., Wang, C., Song, Y., Chen, H., Xu, Y., 2014. Activity of Ni–Cu–Al based catalyst for renewable hydrogen production from steam reforming of glycerol. Energy Conversion and Management, 78, 253-259.

Elias, KFM., Lucredio, AF., Assaf, EM., 2013. Effect of CaO addition on acid properties of Ni-Ca/Al_2O_3 catalysts applied to ethanol steam reforming. International Journal of Hydrogen Energy 38, 4407-4417.

Fan, M.S., Abdullah, A.Z., Bhatia, S., 2011. Hydrogen production from carbon dioxide reforming of methane over Ni-Co/MgO-ZrO_2 catalyst: process optimization. International Journal of Hydrogen Energy, 36, 4875-4886.

Franchini, C.A., Aranzaez, W., de Farias, A.M.D., Pecchi, G., Fraga, M.A., 2014. Ce-substituted $LaNiO_3$ mixed oxides as catalyst precursors for glycerol steam reforming. Applied Catalysis B: Environmental, 147, 193-202.

Garcıa, V., Fernandez, J.J., Ruız, W., Mondragon, F., Moreno, A., 2009. Effect of MgO addition on the basicity of Ni/ZrO_2 and on its catalytic activity in carbon dioxide reforming of methane. Catalysis Communication, 11, 240-246.

Gnansounou, E., 2008. Assessing the energy vulnerability: case of industrialized countries. Energy Policy 36, 3734-3744.

Goula, M.A., Lemonidou, A.A., Efstathiou, A.M. 1996. Characterization of carbonaceous species formed during reforming of CH_4 with CO_2 over Ni/CaO-Al_2O_3: Catalysts studied by various transient techniques. Journal of Catalysis 161, 626-640.

Hayakawa, T., Harihara, H., Andersen, A.G., Suzuki, K., Yasuda, H., Tsunoda, T., Hamakawa, S., York, A.P.E., Yoon, Y.S., Shimizu, M., Takehira, K., 1997. Sustainable Ni/$Ca_{1-x}Sr_xTiO_3$ catalyst in situ prepared in partial oxidation of methane to synthesis gas. Applied Catalysis A. 149, 391.

Horiuchi, T., Hidaka, H., Fukui, T., Kubo, Y., Horio, M., Suzuki, K., Mori, T., 1998. Applied Catalysis A: General, 167, 195-202.

Hua, W., Jin, L., He, X., Liu, J., Hu, H., 2010. Preparation of Ni/MgO catalyst for CO_2 reforming of methane by dielectric-barrier discharge plasma. Catalysis Communication, 11, 968-972.

Iakovou, E., Karagiannidis, A., Vlachos, D., Toka, A., Malamakis A., 2010. Waste biomass-to-energy supply chain management: A critical synthesis. Waste Management 30(10), 1860–1870.

Jackson, P., 2006. Why the Peak Oil Theory Falls Down: Myths, Legends, and the Future of Oil. CERA, Client Services Cambridge, MA, USA.

Jakobsson, K., Bentley, R., Soderbergh, B., Aleklett, K., 2012. The end of cheap oil: Bottom-up economic and geologic modeling of aggregate oil production curves. Energy Policy 41, 860-870.

Jiménez-González, C., Boukha, Z., de Rivas, B., Delgado, J.J., Cauqui, M.A., González-Velasco, J.R., Gutiérrez-Ortiz, J.I., López-Fonseca, R., 2013. Structural characterisation of Ni/alumina reforming catalysts activated at high temperatures. Applied Catalysis A: General, 466, 9-20.

Juan-Juan, J., Roman-Martınez, M.C., Illan-Gomez, M.J. 2009. Nickel catalyst activation in the carbon dioxide reforming of methane: Effect of pretreatments. Applied Catalysis A 355, 27-32.

Koo, K.Y., Roh, H/S., Seo, Y/T., Seo, D.J., Yoon, W.L., Park, S.B. 2008. Coke study on MgO-promoted Ni/Al_2O_3 catalyst in combined H_2O and CO_2 reforming of methane for gas to liquid (GTL) process. Applied Catalysis A: General, 340, 183-190.

Laherrere, J., 2003. Will the natural gas supply meet the demand in North America? International Journal of Global Energy 19, 1-62.

Larimi, A.S., Alavi, S.M., 2012. Ceria-zirconia supported Ni catalysts for partial oxidation of methane to synthesis gas. Fuel, 102, 366-371.

Li, D., Nakagawa, Y., Tomishige, K., 2011. Methane reforming to synthesis gas over Ni catalysts modified with noble metals. Applied Catalysis A: General, 408, 1-24.

Liu, D., Quek, X.Y., Cheo, W.N.E., Lau, R., Borgna, A., Yang, Y., 2009. MCM-41 supported nickel-based bimetallic catalysts with superior stability during carbon dioxide reforming of methane: effect of strong metal–support interaction. Journal of Catalysis, 266, 380-390.

Martinez, R., Romero, E., Guimon, C., Bilbao, R., 2004. CO_2 reforming of methane over coprecipitated Ni-Al catalysts modified with lanthanum. Applied Catalysis A: General, 274, 139-149.

Mathews, A.P., 2014. Renewable energy technologies: panacea for world energy security and climate change? Procedia Computer Science 32, 731–737.

Maugeri, L., 2004. Oil: Never cry wolf - Why the petroleum age is far from over. Science 304, 1114-1115.

Melchor-Hernández, C., Gómez-Cortés, A., Díaz, G., 2013., Hydrogen production by steam reforming of ethanol over nickel supported on La-modified alumina catalysts prepared by sol–gel. Fuel, 107, 828-835.

Mette, K., Kühl, S., Tarasov, A., Düdder, H., Kähler, K., Muhler, M., Schlögl, R., Behrens, M., 2015. Redox dynamics of Ni catalysts in CO_2 reforming of methane. Catalysis Today, 242, 101-110.

Nieva, M.A., Villaverde, M.M., Monzón, A., Garetto, T.F., Marchi, A.J., 2014. Steam-methane reforming at low temperature on nickel-based catalysts. Chemical Engineering Journal, 235, 158-166.

Nikoo, M.K., Amin, N.A.S., 2011. Thermodynamic analysis of carbon dioxide reforming of methane in view of solid carbon formation, Fuel Processing Technology, 92, 678–691.

Noor, Z.Z., Yusuf, R.O., Abba, A.H., Abu Hassan, M.A., Mohd Din, M.F. 2013. An overview for energy recovery from municipal solid wastes (MSW) in Malaysia scenario. Renewable and Sustainable Energy Reviews, 20, 378-384.

Odell, P.R., 2010. The long-term future for energy resources' exploitation. Energy & Environment 21, 785-802.

Poeschl, M., Ward, S., Owende, P., 2010. Prospects for expanded utilization of biogas in Germany. Renewable and Sustainable Energy Reviews, 14, 1782-1797.

Provendier, H., Petit, C., Estournès, C., Libs, S., Kiennemann, A., 1999. Stabilisation of active nickel catalysts in partial oxidation of methane to synthesis gas by iron addition, Applied Catalysis A. 180, 163-173.

Radetzki, M., 2010. Peak Oil and other threatening peaks - Chimeras without substance. Energy Policy 38, 6566-6569.

Ranjbar, A., Rezaei, M., 2012. Preparation of nickel catalysts supported on $CaO.2Al_2O_3$ for methane reforming with carbon dioxide. International Journal of Hydrogen Energy, 37, 6356-6362.

Rezaei, M., Alavi, S.M., Sahebdelfar, S., Bai, P., Liu, X., Yan, Z.F., 2008. CO_2 reforming of CH_4 over nanocrystalline zirconia-supported nickel catalysts. Applied Catalysis B: Environmental, 77, 346-354.

Roh, H.S., Jun, K.W., 2008. Carbon dioxide reforming of methane over Ni catalysts supported on Al_2O_3 modified with La_2O_3, MgO and CaO. Catalysis Survey Asia, 12, 239-252.

Ross, M.L., 2001. Does oil hinder democracy? World Politics 53, 325-361.

Rutherford, J.P., Scharpf, E.W., 2007. Carrington CG. Linking consumer energy efficiency with security of supply. Energy Policy 35, 3025-3035.

Sahira, M.H., Qureshi, A.H., 2007. Specific concerns of Pakistan in the context of energy security issues and geopolitics of the region. Energy Policy 35, 2031-2037.

Sahli, N., Petit, C., Roger, A.C., Kiennemann, A., Libs, S., Bettahar, M.M., 2006. Ni catalysts from $NiAl_2O_4$ spinel for CO_2 reforming of methane. Catalysis Today 113, 187-193.

Seung-hoon, K., Jae-sun, J., Eun-hyeok, Y., Kwan-Young, L., Ju, M.D., 2014. Hydrogen production by steam reforming of biomass-derived glycerol over Ni-based catalysts. Catalysis Today, 228, 145-151.

Simmons, M., 2007. Is the world supply of oil and gas peaking? International Petroleum Week 2007, February 13, London.

Solomon, K.R., Lora, E.E.S., 2009. Estimate of the electric energy generating potential for different sources of biogas in Brazil. Biomass and Bioenergy 33, 1101–1107.

Son, I.H., Lee, S.J., Roh, H.S., 2014. Hydrogen production from carbon dioxide reforming of methane over highly active and stable MgO promoted Co-Ni/γ-Al_2O_3 catalyst. International Journal of Hydrogen Energy, 39, 3762-3770.

Sovacool, B.K., Mukherjee, I., 2011. Conseptualising and measuring energy security: A synthesized approach. Energy 36, 5343-5355.

Stegen, K.S., 2011. Deconstructing the ‘‘energy weapon’’: Russia’s threat to Europe as case study. Energy Policy 39, 6505-6513.

Tao, K., Zhang, Y., Terao, S., Tsubaki, N., 2010. Development of platinum-based bimodal pore catalyst for CO_2 reforming of CH_4. Catalysis Today 153, 150-155.

Usman, M., Daud, W.W.M.A., Abbas H.F., 2015. Dry reforming of methane: Influence of process parameters: A review. Renewable and Sustainable Energy Reviews, 45710-744

van der Pol, T.D., van Lerland, E.C., Gabbert, S., Weikard, H.P., Hendrix, E.M.T., 2015. Impacts of rainfall variability and expected rainfall changes on cost-effective adaptation of water systems to climate change. Journal of Environmental Management 154, 40–47

Winzer, C., 2012. Conceptualizing energy security. Energy Policy, 46, 36-48.

Wiréhn, L., Danielsson, A., Simone, T., Neset, S., 2015. Assessment of composite index methods for agricultural vulnerability to climate change. Journal of Environmental Management 156, 70–80

Xu, J.J., Zhou, W., Li, Z., Wang, J., Ma, J., 2009. Biogas reforming for hydrogen production over nickel and cobalt bimetallic catalysts. International Journal of Hydrogen Energy 34, 6646-6654.

Xu, L., Song, H., Chou, L., 2013. Ordered mesoporous MgO-Al_2O_3 composite oxides supported Ni based catalysts for CO_2 reforming of CH_4: Effects of basic modifier and mesopore structure. International Journal of Hydrogen Energy, 38, 7307-7325.

Yang, R., Xing, C., Lv. C., Shi, L., Tsubaki, N., 2010. Promotional effect of La_2O_3 and CeO_2 on Ni/gamma-Al_2O_3 catalysts for CO_2 reforming of CH_4. Applied Catalysis A: General, 385, 92-100.

Yasyerli, S., Filizgok, S., Arbag, H., Yasyerli, N., Dogu, G., 2011. Ru incorporated Ni-MCM-41 mesoporous catalysts for dry reforming of methane: effects of Mg addition, feed composition and temperature. International Journal of Hydrogen Energy 36, 4863-4874.

Zhang, Z.X., 2011. China’s energy security, the Malacca dilemma and responses. Energy Policy 39, 7612-7615.

Zhai, X., Ding, S., Liu, Z., Jin, Y., Cheng, Y., 2011. Catalytic performance of Ni catalysts for steam reforming of methane at high space velocity. International Journal of Hydrogen Energy, 36, 482-489.